Theory and Modeling of Under-Critical Millimeter-Wave Discharge in Atmospheric Air Induced by High-Energy Excited Neutral-Particles Carried via Photons

Yusuke Nakamura[1], Kimiya Komurasaki[2]
[1]Department of Aerospace Engineering, Nagoya University, Furo-cho, Chikusa, Nagoya, 474-8603, Japan
[2]Department of Aeronautics and Astronautics, The University of Tokyo, Hongo 7-3-1, Bunkyo, Tokyo, 113-8656, Japan

Abstract

Past experiments have shown an ionization front propagation in the millimeter-wave whose intensity was one order lower than the critical intensity of breakdown. Propagation in such a low-intensity region is inexplicable by past theories because no mechanism can enhance ionization sufficiently in the precursor region ahead of bulk plasma. This study examines a new propagation theory incorporating excited neutral particles. The excited neutral particles are carried to the precursor region repeating radiative decay and reabsorption of a photon created by that decay process. Ionization occur with collisions of an electron and that excited neutral particle. One-dimensional computations were conducted for various power densities of an incident beam to reproduce propagation. The obtained propagation velocities were around 50% of experimental values for quenching frequencies lower than 10^6 /s.

I. Introduction

Past millimeter-wave discharge experiments conducted in atmospheric air demonstrated that an ionization front propagated toward the millimeter-wave source after the ignition [1--4]. An application of this phenomenon has been proposed for launch vehicles [5,6]. The observed propagation velocities for various incident millimeter-wave beam intensities are shown in Figure 1. In an experiment conducted by Hidaka et al. [1,2] using a millimeter-wave with wavelength λ of 2.73 mm, the incident beam is focused by a lens. In these studies, ionization front propagation from the beam waist, at which plasma was ignited, was observed as it is shown in Figure 2 (a). The beam intensity at the beam waist, with diameter of 5 mm, was greater than 25 GW/m^2, which is higher than the critical intensity of breakdown: [7] 15 GW/m^2, at which increasing effects of electrons exceed decreasing effects. However, in the experiment conducted by Oda et al. [3,4] using a millimeter-wave with wavelength λ of 1.76 mm, an ionization front propagating along a parallel beam from a seed plasma created by an igniter was observed as shown in Figure 2 (b). The incident beam intensity was a few gigawatts per square meter, which is one-order lower than the critical intensity.

To understand the propagation mechanisms, many physical models have been proposed. Numerical reproduction of the propagation was conducted in earlier studies [8--10]. The propagation velocity computed using these models is shown on Figure 1. One of these models is an electron diffusion model proposed by Nam and Verboncoeur [8]. According to this model, electrons diffusing to a precursor region ahead of the plasma are heated by the millimeter wave. Ionizations occur with the collisions between this heated electron and a neutral particle. This model was developed by Boeuf et al. [9] using an effective diffusion coefficient. The ionization-front propagation at over-critical intensity was reproduced. However, propagation at intensity lower than the discharge critical intensity cannot be reproduced using this model because the electrons are not heated sufficiently for ionization. To elucidate propagation at under-critical intensity, Takahashi et al. [10] combined the electron diffusion model with a compressible flow of neutral particles and conducted two-dimensional computations. These computations at under-critical intensity reproduced the gas expansion behind a blast wave produced a higher reduced-electric-field. Therefore, high electron temperature sufficient for ionization was achieved. However, the computed propagation velocities around 10 GW/m^2 were more than one-order slower than that predicted from the experimentally obtained results. Dependence on the incident beam intensity was also very different from that found in the experiments. Furthermore, the propagation in the millimeter wave with intensity of a few gigawatts per square meter, which is the intensity range of Oda's experiment, cannot be reproduced with that model. In this study, a new propagation theory was proposed. Then one-dimensional computations were conducted by modeling of this theory.

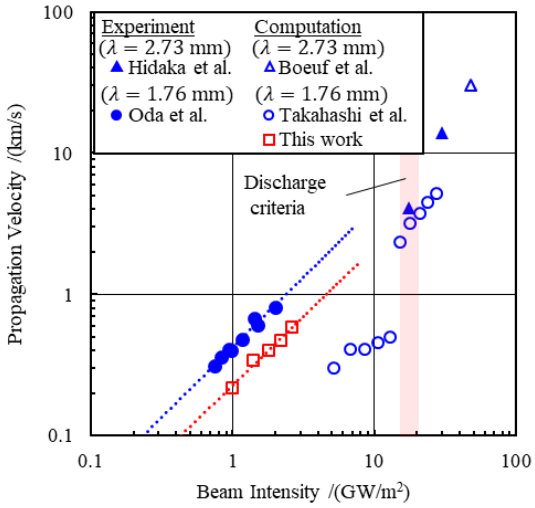

FIG. 1. Measured ionization-front propagation velocity [1--4] and computed velocity [9,10].

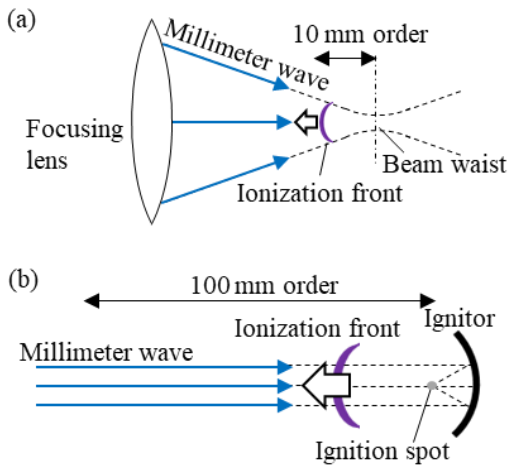

FIG. 2. Schematic images of the experiment conducted in the over-critical condition (a) [1,2] and the under-critical condition (b) [3,4].

A similar propagation phenomenon was also observed in the discharge experiment using microwaves and lasers [11--15], and the propagation mechanisms were discussed [16--19]. However, the same mechanisms cannot be applied for the millimeter-wave discharge because of the differences in plasma structures and propagation velocities. Therefore, explaining the ionization-front propagation in the millimeter-wave of the under-critical intensity requires identification of a physical phenomenon that has not been considered.

II. Ionization-Front Propagation Theory

In this section, what determine the propagation velocity of the ionization front will be discussed. In the electron diffusion model [8,9], a continuity equation for an electron number density n_e is formed as shown below using electron diffusion coefficient D and net ionization frequency f_i.

$$\frac{\partial n_e}{\partial t} - D\Delta n_e = S = f_i n_e \qquad (1)$$

In that equation, D takes a value close to an electron free diffusion coefficient D_e at the edge of ionization front at which the electron number density is extremely low, although it takes a value of an ambipolar diffusion coefficient D_a of a bulk plasma. The propagation velocity derived from this equation is known to be $2\sqrt{Df_i}$. If that value is different in terms of position, the velocity obeys its maximum [20]. An earlier computational study of the over-critical condition [9] showed that the computational propagation velocity was found in a region where the electrons diffuse freely because both D and f_i took maximum values there. In the under-critical case, something that increases ionization is needed for propagation. $2\sqrt{Df_i}$ can take its maximum value near the bulk plasma in which the electron's diffusion is ambipolar if something in the bulk plasma increases the ionization frequency sufficiently. The experimental propagation velocity U_{ion} is 1 km/s when the intensity of an incident millimeter-wave S_{MMW} is 2.5 GW/m^2. In this case, if the diffusion coefficient is $D_a \cong 1\times10^{-3}\ \mathrm{m^2/s}$ at the position deciding the propagation velocity, then a net ionization frequency f_i is expected to be $3\times10^8\ /\mathrm{s}$ at that position. Here, it was assumed that the electron temperature is around 1 eV. The energy used by one electron per unit times for collisional ionization $\varepsilon_i f_i$ is $5\times10^9\ \mathrm{eV/s}$ when $\varepsilon_i = 15.6\ \mathrm{eV}$, which is the ionization energy of a nitrogen molecule. However, the energy absorbed by one electron with inverse bremsstrahlung is $6\times10^{10}\ \mathrm{eV/s}$, whereas a momentum transfer frequency of electrons is $2\times10^{12}\ /\mathrm{s}$. Therefore, the 8% of absorbed energy goes to net ionization. That energy ratio is the value at the bulk but the total energy ratio is thought to take a similar value because most of the energy absorption occurs in the bulk plasma. Assuming that, the maximum electron number density can be derived from the following equation.

$$\frac{0.08\times S_{MMW}}{U_{ion}\varepsilon_i} = 8\times10^{22}\ /\mathrm{m^3} \qquad (2)$$

That density is so high that most of the incident beam energy is reflected at the plasma surface because that is two or three orders higher than the cutoff density of collisional plasma [21]. However, such reflection has never been observed in past discharge experiments. That fact suggests that the position determining the propagation velocity is not in the bulk plasma in which the diffusion coefficient is D_a. The net ionization frequency needed to realize the experimental propagation velocity can take more capable value if the diffusion coefficient is D_e at the position deciding the velocity. From the discussion presented above, one can infer that the position deciding the velocity is at a precursor ahead of the ionization front in which electron number density is sufficiently small that the diffusion coefficient is close to D_e.

A phenomenon which is important for the propagation should be able to affect the precursor and increase the ionization frequency. One of such phenomena is that a photon coming from the bulk plasma directly ionizes a neutral particle at the precursor, which is called photoionization. This phenomenon is mainly discussed in the field of streamer discharges and some behavior of the streamer head was explained by a model considering some photoionization processes [22,23] while the typical propagation velocity of the streamer head is more than two orders faster than the velocity of the ionization front discussed in this study. The photoionization effect depends only on the bulk condition and, generally, becomes stronger with higher electron temperature at the bulk. While the electron temperature considered in the computational research on the propagation in the over-critical condition [9] is 2 eV, discussions in a previous spectroscopic research on the under-critical condition [24] suggested that plasma around the radiation source is in local thermodynamic

equilibrium (LTE) and the electron temperature at there is lower than 1 eV. Because the propagation in over-critical condition can be well explained with a model without photoionization [9,10], it is unlikely that the photoionization begins to be effective in the under-critical condition with weaker intensity of millimeter-wave beam. Therefore, in this study, it was assumed that the photoionization effect is negligibly small, and another photonic effect which increases the ionization frequency was considered. The ionization frequency can be increased by electronically excited neutral particles. However, the excited neutral particles cannot be created sufficiently in the precursor because the electron number density is very small there, whereas these particles are created by collisions between an electron and a neutral particle. Despite that, the excited neutral particles can exist in the precursor if they are transferred from the bulk plasma via photons. The schematic images of the transfer processes proposed in this study are shown in Figure 3. The high-energy electronically excited species created at the bulk plasma by collision between an electron and a neutral particle quickly decay to the ground state in the time scale of 10^{-10} s, thereby creating a photon. The photon is reabsorbed by a neutral particle in the ground state after traveling a short distance, recreating the excited species. Repeating these processes, the excited neutral particles are transferred to the precursor region. The ionization with this process can be more effective in the slower ionization-front having longer characteristic time because it takes time to carry enough excited neutral particles to the precursor. In this study, a new propagation mechanism in which the high-energy electronically excited neutral particle play an important role was proposed. The possibility of the propagation with this mechanism was discussed with one-dimensional computation using a simple model.

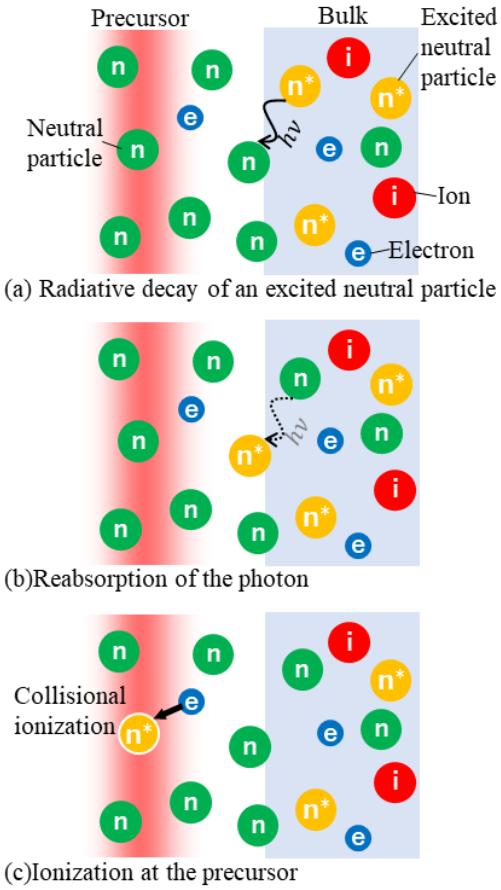

FIG. 3. Schematic images of the excited neutral-particle transfer process. Excited neutral particles are carried to the precursor by repeating the process (a) and (b), and ionize with the collision (c).

III. Computational Models and Methods

To produce a computational model, the following five assumptions were used for simplicity. (1) The only air components are nitrogen molecules. The previous experimental results in the over-critical condition [2] suggested that there is no big difference between the propagation velocity in air and that in the pure nitrogen. (2) Motions of neutral particles, which are nitrogen molecules, are negligibly small compared to the ionization front. (3) The energy distribution of electrons obeys a Boltzmann distribution determined by the electron temperature T_e. (4) The energy distribution of vibrational excitations obey a Boltzmann distribution determined by the vibrational temperature T_v. (5) Energy distribution of electronic excitation except ground state obeys a Boltzmann distribution determined by the electron temperature at bulk plasma $(T_e)_B$ because most of the electronically excited neutral particles derive from the bulk. For that reason, the number densities of the electronically excited neutral particles with excitation level i, which is described as $n^*_{n,i}$, obey the following equations.

$$n^*_{n,i} = \frac{n^*_n}{Z_{ex}} \exp\left(-\frac{\epsilon_i}{(T_e)_B}\right) \quad (3)$$

In that equation, the number density of all the electronically excited neutral particles n_{n}^{*} and a partition function Z_{ex} are defined as shown below.

$$n_{\mathrm{n}}^{*} \equiv \sum_{i\neq 0} n_{\mathrm{n},i}^{*} \qquad Z_{\mathrm{ex}} \equiv \sum_{i\neq 0} \exp\left(-\frac{\epsilon_i}{(T_{\mathrm{e}})_{\mathrm{B}}}\right) \tag{4}$$

The most important part of the propagation mechanism proposed herein is transportation of the excited neutral particles by photon. Assuming that the photon created with a radiative decay of an excited neutral particle is not absorbed except in the reabsorption process recreating an excited neutral particle, the photoexcitation rate at arbitral point $\boldsymbol{r}$ caused by photons created by the decay process at point $\boldsymbol{r}'$, which described as $S_{\boldsymbol{r}}(\boldsymbol{r}')$, is expressed as follows.

$$S_{\boldsymbol{r}}(\boldsymbol{r}') = \frac{\kappa A_{\mathrm{Ei}} n_{\mathrm{n}}^{*}\left(\boldsymbol{r}^{'}\right)\exp\left(-\kappa|\boldsymbol{r}-\boldsymbol{r}'|\right)}{4\pi(\boldsymbol{r}-\boldsymbol{r}')^2} \tag{5}$$

In that expression, A_{Ei} and κ respectively denote Einstein's A coefficient, which is the frequency of radiative decay, and an absorption coefficient of the photons. Net photoexcitation rate at the point $\boldsymbol{r}$ can be obtained by integrating $S_{\boldsymbol{r}}$ over the entire region where photons can come from and subtracting the number of decays at the point $\boldsymbol{r}$ from it. A photon created from a radiative decay of a high-energy excited particle, which is important for ionization, is reabsorbed with a mean free path of around 10^{-5} m [25]. That is much smaller than the typical scale of an ionization front of approximately 10^{-4} m [26]. In such a case, the increased amount of a number density of excited neutral particles at an arbitrary point is described as the following, considered until the second order of Taylor expansion.

$$\frac{A_{\mathrm{Ei}}}{3\kappa^2}\frac{\partial^2 n_{\mathrm{n}}^{*}}{\partial z^2} \tag{6}$$

Using the approximation presented above, a continuity equation of a number density of excited neutral particles can be presented as the following diffusion-form equation.

$$\frac{\partial n_{\mathrm{n}}^{*}}{\partial t} - D_{\mathrm{ex}}\frac{\partial^2 n_{\mathrm{n}}^{*}}{\partial z^2} = S_{\mathrm{ex}} \qquad D_{\mathrm{ex}} \equiv \frac{A_{\mathrm{Ei}}}{3\kappa^2} \tag{7}$$

Therein, S_{ex} is a source term of the excited neutral particles. According to an earlier study of the excited fluorescence [27] and absorption coefficient [25] of a photon, typical values of A_{Ei} and κ for the excited neutral particles for which the excitation energy is higher than 13 eV are around 10^{10} /s and 10^{5} /m, respectively. Therefore, D_{ex} for such high-energy excited neutral particles are on the order of $1\ \mathrm{m}^2/\mathrm{s}$. For the present study, it was assumed that the values of D_{ex} are the same, which is on the order of $1\ \mathrm{m}^2/\mathrm{s}$, irrespective of the excitation states for simplicity. Although that is not real, this assumption is sufficient for discussing the possibility of the propagation mechanism because the density of the high-energy excited neutral particle, which is important for ionization at least, was close to the real value with this assumption. The following equation was used to compute the source term of the excited neutral particles S_{ex}.

$$\begin{aligned} S_{\mathrm{ex}} = {} & n_{\mathrm{e}} n_{\mathrm{n},0}^{*}\sum_{i\neq 0} K_{0,i} - n_{\mathrm{e}}\sum_{i\neq 0} n_{\mathrm{n},i}^{*} K_{i,0} \\ & - n_{\mathrm{e}}\sum_{i} n_{\mathrm{n},i}^{*} K_{i,\mathrm{ion}} + {n_{\mathrm{e}}}^{3}\sum_{i} r_i - \nu_{\mathrm{q}} n_{\mathrm{n}}^{*} \end{aligned} \tag{8}$$

In this source term, excitations from the ground state to an excitation level i, deexcitations from an excitation level i, ionizations from an excitation level i, and three-body recombination to an excitation level i were considered, whereas $K_{0,i}$, $K_{i,0}$, $K_{i,\mathrm{ion}}$, and r_i respectively denote the reaction rate coefficients for the reactions. Also, $n_{\mathrm{n},0}^{*}$ and $n_{\mathrm{n},i}^{*}$ respectively represent the number densities of the neutral particles on the ground state and a number density of the neutral particle on the excitation level of i. The last term of Eq. (8) is the term of quenching or other decay process of the excited neutral particles without radiation. Decay with radiation is included in the diffusion term of Eq. (7). This quenching frequency depends on the excited species. It is difficult to estimate especially for high-energy excited species. Therefore, the model was discussed while ignoring quenching term first. The range of the quenching frequency with which the discussion presented above is applicable was sought from the computation changing that frequency.

To ascertain the electron number density, the following diffusion equation was used.

$$\frac{\partial n_{\mathrm{e}}}{\partial t} - D_{\mathrm{eff}}\frac{\partial^2 n_{\mathrm{e}}}{\partial z^2} = f_{\mathrm{i}} n_{\mathrm{e}} \tag{9}$$

Therein, D_{eff} is an effective diffusion coefficient as the following proposed in past research [9].

$$D_{\mathrm{eff}} = \frac{\alpha D_{\mathrm{e}} + D_{\mathrm{a}}}{\alpha + 1} \qquad \alpha \equiv \frac{{\lambda_{\mathrm{D}}}^2}{L^2} \tag{10}$$

In those equations, λ_{D} and L respectively represent the Debye length and the scale length of the ionization front. The ionization frequency was derived from the following equation, considering the collisional ionization, two-body recombination, and three-body recombination.

$$\begin{aligned} f_{\mathrm{i}} = {} & n_{\mathrm{n},0}^{*} K_{0,\mathrm{ion}} + \sum_{i\neq 0} n_{\mathrm{n},i}^{*} K_{i,\mathrm{ion}} \\ & - n_{\mathrm{e}} r_{2\mathrm{B}} - {n_{\mathrm{e}}}^{2}\sum_{i} r_i \end{aligned} \tag{11}$$

Therein, r_{2B} represents the reaction rate constant of two-body dissociative recombination.

The rate coefficient for the reactions between an electron and a neutral particle in its ground state was obtained by convolution integration of the electron-energy distribution function determined by the electron temperature and the cross section obtained from the database [28], whereas rate coefficients for ionizations of an excited neutral particle were derived from a classical approximation equation [29]. The coefficient of electron collisional deexcitation and three-body recombination were determined to satisfy Saha-Boltzmann equation in the case of thermal equilibrium. The two-body recombination coefficient was determined as follows referring to the previous study [30,31].

$$r_{2B} = 10^{-13}\left(\frac{300\ \mathrm{K}}{T_e}\right)^{0.5}\ \mathrm{m^3/s} \qquad (12)$$

Although that is a rough estimation, that is enough to evaluate the propagation velocity because recombination is not effective in the precursor with a low electron number density but behind the ionization front at which the number density starts decreasing.

To compute the electromagnetic field, Maxwell's equations were used.

$$\frac{\partial H_x}{\partial z} = \varepsilon_0\frac{\partial E_y}{\partial t} + J_e \qquad (13)$$

$$\frac{\partial E_y}{\partial z} = \mu_0\frac{\partial H_x}{\partial t} \qquad (14)$$

These equations were coupled with the following motion equation of electrons.

$$\frac{\mathrm{d}J_e}{\mathrm{d}t} = \frac{e^2 n_e}{m_e}E_y - \nu_m J_e \qquad (15)$$

The root mean square values of the electric field E_{rms} were derived for each period of the incident millimeter wave. Energy absorbed by an electron per unit time s_{abs} was derived from the following equation.

$$s_{abs} = \frac{e^2 {E_{rms}}^2 \nu_m}{m_e(\omega^2 + {\nu_m}^2)} \qquad (16)$$

The electron temperature in each cell was found assuming the energy balance described as following equation.

$$s_{abs}n_e = \frac{3}{2}k_B T_e\frac{\partial n_e}{\partial t} + \epsilon_{ex} + \epsilon_v + \epsilon_{ion} + \epsilon_{el} \qquad (17)$$

Therein, ϵ_{ex}, ϵ_v, ϵ_{ion}, and ϵ_{el} are the energy going to the electronic excitation, the vibrational excitation, the ionization, and the translational energy of heavy particles with elastic collisions, respectively.

The timestep and mesh size were found considering the mesh-convergence result. The computations were conducted on a one-dimensional domain of which the length was set to 8λ. PML boundary conditions were used as absorption boundaries placed at both edges of the domain. The initial plasma, the electron number density, and the vibrational excitation energy were given in a Gaussian spot where the peak position was 0.5λ from the boundary opposite to the millimeter wave incident direction. The ionization front propagating from this initial plasma toward the beam source was computed. The computations were conducted by changing the incident beam intensity for various D_{ex}.

IV. Results and Discussion

Figure 4(a) shows distributions of the electron number density and electron temperature after $14.1\ \mu\mathrm{s}$ from the initial value obtained in the calculation with $D_{ex} = 2\ \mathrm{m^2/s}$ and the incident beam intensity of $2.2\ \mathrm{GW/m^2}$. The electron number density increased gradually from the initial value. Propagation bulk-plasma having electron number density and electron temperature of around $3\times10^{21}\ \mathrm{/m^3}$ and 1 eV, respectively, was formed after approximately $3\ \mu\mathrm{s}$. The propagation velocities obtained from the calculation changing incident-beam intensity from $1.0\ \mathrm{GW/m^2}$ to $2.6\ \mathrm{GW/m^2}$ by $0.4\ \mathrm{GW/m^2}$ are shown in Figure 1. The propagation velocity was about 50% of the experimental value, irrespective of the incident beam intensity. It showed very good agreement compared with values calculated in earlier studies. Figure 4(b) portrays distributions of D_{eff}, f_i, and $2\sqrt{D_{eff}f_i}$ around the ionization front. Also, f_i maintained a high value until D_{eff} approached an electron-free diffusion D_e with waving attributable to the influence of a standing wave of a millimeter wave. Results show that $2\sqrt{D_{eff}f_i}$ was maximized near the boundary where diffusion becomes D_e, forming a precursor that determines the propagation velocity.

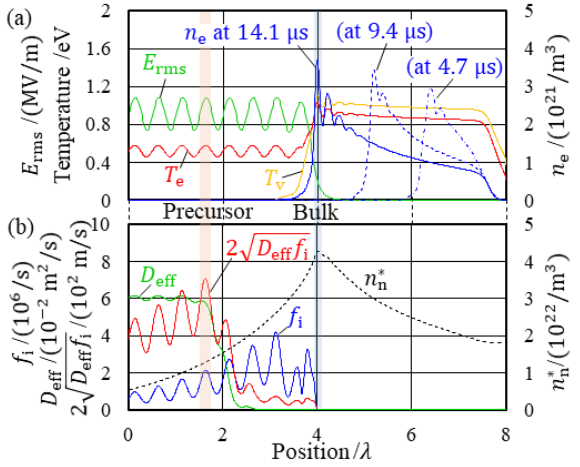

FIG. 4. (a) The time evolution of n_e distribution and distributions of E_{rms}, T_e and T_v at $14.1\ \mu\mathrm{s}$ from the

initial value. (b) Distribution of f_i, D_{eff}, $2\sqrt{D_{eff}f_i}$ and n_n^* at 14.1 μs from the initial value.

Next, the dependence of D_{ex} on the propagation was examined using calculations changing D_{ex} from 0.2 m^2/s to 2.6 m^2/s. The obtained computational velocities normalized by the experimental velocities are shown in Figure 5(a). When D_{ex} is greater than 0.6 m^2/s, the propagation velocities were approximately 50% of the experimental values irrespective of the incident beam intensity, but when they were less than this, the velocity was markedly lower. Moreover, as D_{ex} becomes smaller, the $\lambda/4$ structure attributable to the standing wave becomes increasingly prominent. The propagation velocity became almost constant at large D_{ex} because the number density of the excited neutral particles at the precursor hardly increased when the scale length of that number density distribution reaches the length between the precursor and the bulk due to large D_{ex}.

To investigate the influence of de-excitation caused by quenching or other effects including collisional reaction between heavy particles and dissociation, the quenching frequency ν_q was changed from 10^5 /s to 10^7 /s. Moreover, D_{ex} was fixed at 2 m^2/s. The propagation velocities obtained from these computations are presented in Figure 5(b). When the quenching frequency was lower than 10^6 /s, the propagation velocity retained its value at 50% of the experimental value, but when the frequency was greater, the velocity drops gradually to about 30% at the frequency of 10^7 /s.

The numerical results above demonstrate that the ionization front propagation with velocity of around 50% of the experimental value can be reproduced using the proposed mechanism. Although the result is better than results obtained using earlier models, still 50% difference exists. This difference is thought to derive from simplification of the model or the energy concentration because of the ionization front structure. Therefore, modifications of the model or multi-dimensional computations must be made to eliminate this difference.

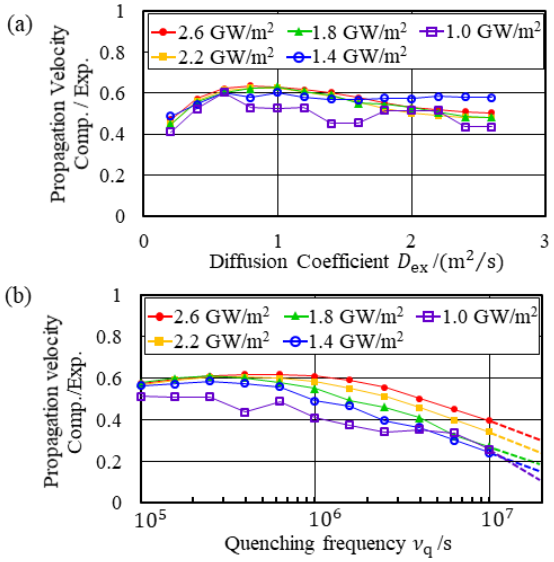

FIG. 5. (a) Ionization front propagation velocities normalized by experimental velocity for various D_{ex} (b) and for various ν_q.

V. Conclusion

A new mechanism of an ionization front propagation in an under-critical millimeter-wave beam was proposed in this study. The high-energy excited particles transported by photons form a bulk driving the propagation. This mechanism was simply modeled. The propagation with this mechanism was simulated numerically. The propagation velocities obtained from this computation were around 50% of the experimental value when the quenching frequency was lower than 10^6 /s. Compared with computational results obtained using past models, that value showed good agreement with results obtained from experimentation.

This work was supported by JSPS Grants-in-Aid for Scientific Research: Grant Nos. JP15H0577 and JP17J09280.

[1] Y. Hidaka, E. M. Choi, I. Mastovsky, M. A. Shapiro, J. R. Sirigiri, and R. J. Temkin, Physical Review Letters **100** 035003 (2008).
[2] Y. Hidaka, E. M. Choi, I. Mastovsky, M. A. Shapiro, J. R. Sirigiri, R. J. Temkin, G. F. Edmiston, A. A. Neuber, and Y. Oda, Physics of Plasmas **16** 055702 (2009).
[3] Y. Oda, K. Komurasaki, K. Takahashi, A. Kasugai, and K. Sakamoto, Journal of Applied Physics **100** 113307 (2006).
[4] Y. Oda, K. Kajiwara, K. Takahashi, A. Kasugai, K. Sakamoto, and K. Komurasaki, Japanese Journal of Applied Physics **48** 116001 (2009).
[5] T. Nakagawa, Y. Mihara, and K. Komurasaki, Journal of Spacecraft and Rockets **41**(1) 151 (2004).
[6] M. Fukunari, K. Komurasaki, A. Arnault, and T. Yamaguchi, Applied Optics **53** I16 (2014).
[7] A. D. MacDonald, Microwave Breakdown in Gases, Willey, 1966.
[8] S. K. Nam and J. P. Verboncoeur, Physical Review

Letters **103** 055004 (2009).
[9] J. P. Boeuf, B. Chaudhury, and G. Q. Zhu, Physical Review Letters **104** 015002 (2010).
[10] M. Takahashi, Y. Kageyama, and N. Ohnishi, AIP Advances **7**(5) 055206 (2017).
[11] K. V. Khodataev, Journal of Propulsion and Power **24**(5) 962 (2008).
[12] I. I. Esakov, L. P. Grachev, and K. V. Khodataev, AIAA Aerospace Sciences Meeting Exhibition, AIAA2007-433, 2007.
[13] P. Bournot, P. A. Pincosy, G. Inglesakis, M. Autric, D. Dufresne, and J. P. Caressa, Acta Astronautica, **6(**3-4) **257** (1979).
[14] I. A. Bufetov, A. M. Prokhorov, V. B. Fedorov, and V. K. Fomin, JETP Letters **39** 258 (1984).
[15] K. Matsui, T. Shimano, J. A. Ofosu, K. Komurasaki, T. Schoenherr, and H. Koizumi, Vacuum **136** 171 (2016).
[16] K. V. Khodataev, 44th AIAA Aerospace Sciences Meeting Exhibition, AIAA2016-789, 2016.
[17] S. A. Ramsden and P. Savic, Nature **201**(4951) 1217 (1964).
[18] Y. P. Raizer, Soviet Physics Jetp **21**(5) 1009 (1965).
[19] K. Shimamura, K. Komurasaki, J. A. Ofosu, and H. Koizumi, IEEE Transactions on Plasma Science **42(**10) 3121 (2014).
[20] U. Ebert, W. vanSaarloos, and C. Caroli, Physical Review E **55** 1530 (1997).
[21] W. Woo and J. S. DeGroot, Physics of Fluids, **27** 475 (1984).
[22] J Stephens, M. Abide, A. Fierro, and A. Neuber, Plasma Sources Science and Technology, **27** 075007 (2018).
[23] B. Bagheri, and J. Teunissen, Plasma Sources Science and Technology, **28** 045013 (2019).
[24] K. Tabata, Y. Harada, Y. Nakamura, K. Komurasaki, H. Koizumi, T. Kariya, and R. Minami, Journal of Applied Physics, **127** 063301 (2020).
[25] R. E. Huffman, Y. Tanaka, and J. C. Larrabee, The Journal of Chemical Physics, **39** 910 (1963).
[26] Y. Nakamura, K. Komurasaki, M. Fukunari, and H. Kouzumi, Journal of Applied Physics **124** 033303 (2018).
[27] C. Y. R. Wu, H. Fung, K. Chang, T. S. Singh, X. Mu, J. B. Nee, S. Chiang, and D. L. Judge, The Journal of Chemical Physics, **127** 084314 (2007).
[28] S. Pancheshnyi, S. Biagi, M. C. Bordage, G. J. M. Hagelaar, W. L. Morgan, A. V. Phelps, and L. C. Pitchford, Chemical Physics, **398** 148 (2012).
[29] M. A. Lieberman and A. J. Lichtenberg, Principles of Plasma Discharges and Materials Processing, Wiley, 2005.
[30] I. A. Kossyi, A. Y. Kostinsky, A. A. Matveyev, and V. P. Silakov, Plasma Sources Science & Technology, **1**(3) 207 (1992).
[31] M. Capitelli, C. M. Ferreira, B. F. Gordiets, and A. I. Osipov, Plasma Kinetics in Atmospheric Gases, Springer, 2000.